

1 This manuscript is a preprint and has been submitted for publication in *Applied Spectroscopy*.
2 Take into consideration that the manuscript has yet to be formally accepted for publication and
3 may have slightly different content between the preprint and accepted version. The final version
4 of this manuscript will be available via the publication DOI link. Please feel free to contact any
5 of the authors.
6

7

8

9

10

11

12

13

14

15

16

17

18

19

20

21

22

23

24 **In-situ quantification of carbonate species concentrations, pH and pCO₂ in calcite fluid**
25 **inclusions using confocal Raman spectroscopy.**

26 Michael Naylor Hudgins ^{a,b*}, Todd K. Knobbe ^a, Julia Hubbard ^a, Andrew Steele ^c, Justin G.
27 Park^{a,b}, and Morgan F. Schaller ^{a,b*}

28 ^a *Department of Earth and Environmental Sciences, Rensselaer Polytechnic Institute, Jonsson*
29 *Rowland Science Center, Troy, NY, USA*

30 ^b *Rensselaer Astrobiology Research and Education Center, Rensselaer Polytechnic Institute,*
31 *Jonsson Rowland Science Center, Troy, NY, USA*

32 ^c *Earth and Planets Laboratory, Carnegie Institution for Science, Washington, DC, USA*

33 *Corresponding Author: schall@rpi.edu

34 *Co-corresponding Author: hudgim@rpi.edu

35 **Abstract**

36 Carbonate minerals are globally distributed on the modern and ancient Earth and are abundant in
37 terrestrial and marine depositional environments. Fluid inclusions hosted by calcite retain
38 primary signatures of the source fluid geochemistry at the time of mineral formation (i.e., pCO₂)
39 and can be used to reconstruct paleoenvironments. Confocal laser Raman spectroscopy provides
40 a quick, non-destructive approach to measuring the constituents of fluid inclusions in carbonates
41 and is a reliable method for qualitatively determining composition in both the aqueous and gas
42 phases. Here, we demonstrate a method for accurately quantifying bicarbonate and carbonate ion
43 concentrations (down to 20 μM) and pH (7-10) from fluid inclusions using confocal Raman
44 spectroscopy. Instrument calibrations for carbonate (CO₃²⁻) and bicarbonate (HCO₃⁻)
45 concentrations and pH were performed using stock solutions. We show that the calcite host
46 mineral does not affect accurate quantification of carbonate solution concentrations or pH
47 determinations, and that these parameters can be used to estimate the pCO₂ of a solution
48 entrapped within a fluid inclusion. We apply the technique to Icelandic spar calcite and find a
49 [CO₃²⁻] = 0.098, [HCO₃⁻] = 0.044, pH = 9.33, and CO₂ (ppm) = 167. The presence of gaseous
50 Raman peaks for CO₂, CH₄, and H₂S suggests that the mineral precipitated in a reducing
51 environment with a similar atmospheric density.

52 **Keywords:** Raman spectroscopy, fluid inclusions, carbonate system, pH, CO₂, quantification

53 **Introduction**

54 Fluid inclusions provide a wealth of information pertaining to a mineral's environment at
55 the time of formation^{1,2}. The ability to quantify the constituents within fluid inclusions provides
56 information on geochemical parameters such as; initial temperature and pressure conditions,
57 salinity, pH, and solution and gas composition of any included gas phases³⁻⁹. These geochemical
58 indicators can be estimated by using Raman spectroscopy, a non-destructive method, that can be
59 applied to the in-situ study of micron-scale fluid inclusions^{6,10-14}.

60 Calcium carbonate minerals are common and abundant in a variety of environmental
61 settings on Earth, ranging from metamorphic carbonates forming in subduction zones¹⁴ to low
62 temperature authigenic marine sediments¹⁵ and surficial deposits (pedogenic or speleothems)^{16,17}.
63 Many of these types of carbonates can contain fluid inclusions, in metamorphic carbonates they
64 have been used to track carbon transport in Earth's interior¹⁴ and in low-temperature carbonates
65 fluid inclusions have been used to measure paleoenvironmental proxies in both the terrestrial and
66 marine realms¹⁵⁻¹⁸. Many studies have focused on carbon and oxygen isotopic compositions of
67 either the mineral matrix or fluid within inclusions¹⁶⁻¹⁹, but relatively fewer studies have
68 investigated the gas concentration or aqueous composition of fluid inclusions in non-diagenetic
69 carbonate minerals^{15,20,21}.

70 A fundamental problem in paleoclimatology is the lack of accurate atmospheric pCO₂
71 estimates prior to the ice core record²². The proxy methods that have been deployed (e.g., the
72 $\delta^{13}\text{C}$ of pedogenic carbonates, leaf stomatal indices, and boron isotopes^{16,23-25}) show similar
73 trends but disagree in absolute value²³⁻²⁹. However, dissolved gases and solutes in the aqueous
74 phase of carbonate mineral fluid inclusions can provide valuable insight into the geochemical
75 conditions of the mineral's formation environment, which can be related back to absolute
76 atmospheric concentrations at the time of precipitation^{1-4,7,30}. Unfortunately, these analyses

77 require the destruction of fluid inclusions during bulk analyses of the released gases and require
78 large sample sizes to enable accurate measurement^{31–33}. In contrast, Raman spectroscopy is a
79 non-destructive method that can provide rapid analyses of liquid and gas phase compositions
80 within individual fluid inclusions^{5,34}. This method enables each of the components of the
81 carbonate system (e.g., $[\text{CO}_3^{2-}]$, $[\text{HCO}_3^-]$, pH, and pCO_2) to be quantified discretely in-situ
82 without disturbing the host mineral matrix. However, before quantification of any molecules
83 measured directly within natural fluid inclusion samples, the mineral system's Raman spectrum
84 and the host mineral's effects on solute quantification need to be evaluated.

85 Identification and quantification of the carbonate species (e.g., CO_3^{2-} , HCO_3^-)
86 concentration provides information on solution pH and pCO_2 of the system that the mineral
87 precipitated in³⁵. In moderately alkaline systems, HCO_3^- is the dominant carbon species in
88 solution, and the Raman signal of HCO_3^- has been observed in alkaline solutions in quartz hosted
89 fluid inclusions^{14,36,37}. However, these studies only recorded the presence of HCO_3^- and did not
90 attempt to quantify the concentration. Although a weak Raman scatterer, detailed studies have
91 shown that HCO_3^- is amenable to quantification over a range of concentrations using Raman
92 spectroscopy^{38–40}. However, these studies did not address the applicability of Raman
93 spectroscopy to quantifying HCO_3^- concentrations in natural samples.

94 In this study, we present a method for the accurate measurement of $[\text{CO}_3^{2-}]$ and $[\text{HCO}_3^-]$
95 in fluid inclusions via Raman spectroscopy and use these measurements to estimate the pCO_2
96 with which the inclusion fluid had equilibrated. We construct calibration curves for CO_3^{2-} and
97 HCO_3^- using Na_2CO_3 and NaHCO_3 solutions via two different methods (with and without the
98 addition of a calcite cover slip to examine the effects of the host mineral)⁴¹, with the ultimate
99 goal of applying these calibrations to natural carbonate samples. We then evaluate the accuracy

100 of each method to determine the most suitable approach for determining the concentration of
101 CO_3^{2-} and HCO_3^- in natural fluid inclusions. We also investigate the effect of increasing solution
102 salinity on the quantification of solutes in fluid inclusions. These studies reveal that [CO_3^{2-}],
103 [HCO_3^-], and the pH of alkaline solutions can be determined using the main Raman bands for
104 CO_3^{2-} and HCO_3^- . The approaches and methods developed in this paper can be applied to a range
105 of fluid inclusions at 1 atm. The specific effects of temperature and pressure broadening on
106 Raman peak parameters of [CO_3^{2-}], [HCO_3^-] are not addressed in this study and has been
107 investigated elsewhere^{42,43}.

108 **Methods**

109 *Calibration Solutions*

110 Prior Raman calibration studies for CO_3^{2-} and HCO_3^- in solution have been made at
111 concentrations spanning from dilute solutions to near saturation ([HCO_3^-]: 1.57-0.0521 molar;
112 [CO_3^{2-}]: 1.55-0.000019 molar)^{38,44,45}. Here, we focus on calibrating the Raman response to CO_3^{2-}
113 and HCO_3^- concentrations in dilute carbonate solutions that are closer to those observed in
114 natural systems (Table 1). We prepared solutions of Na_2CO_3 and NaHCO_3 over a range of [CO_3^{2-}
115], [HCO_3^-], and pH that represent observed concentrations of natural systems^{35,46-52} (Table 1 and
116 2). Natural fluid inclusions in carbonates forming at the surface and in seawater have a range of
117 salinities³. Therefore, we also constructed calibrations over a range of NaCl salinities (1-5 wt%)
118 to more closely resemble natural systems and to investigate salinity effects on the Raman peak
119 response of carbonate species and pH quantification. We consider NaCl calibrations necessary
120 because previous studies have demonstrated that increasing salinity alters the dissociation and
121 solubility constants (K_{co_2} , K_1 , and K_2) and skews the OH^- stretch of H_2O ^{8,53,54}, thus potentially

122 leading to an inaccurate estimation carbonate species concentrations where freshwater calibration
123 curves are applied to saline inclusions.

124 A portion of solutions were equilibrated to the atmosphere and the remainder were
125 prepared as a close system, to encompass a full range of relevant carbonate species
126 concentrations. Desired weights of NaHCO₃, Na₂CO₃, and NaCl were placed in 50 mL centrifuge
127 tubes and continuously mixed with 50 mL of Millipore water (18 Ω) until fully dissolved. Open
128 system solutions were mixed until equilibrium was reached. To obtain a pH <8, 1.2 molar HCl
129 (10% HCl by volume) was added to a 0.25 molar of NaHCO₃ solutions. Once the acid was
130 added, the solution was mixed until a stable pH was reached. Solution temperature and pH were
131 measured with a Thermo Scientific Orion 2-star pH meter before measurement by Raman.

132 To calculate the amount of HCO₃⁻ and CO₃²⁻ in the closed system solutions at the time of
133 measurement, the initial amount of HCO₃⁻ and CO₃²⁻ mixed in the solution was assumed to be
134 equal to the total dissolved inorganic carbon (TDIC). Aqueous speciation of the closed carbonate
135 system were calculated based on measured temperature and pH using the following equations⁵⁵
136 (Eq. 1 and 2):

$$137 \quad [\text{HCO}_3^-] = C_T \frac{K_1[\text{H}^+]}{[\text{H}^+]^2 + K_1[\text{H}^+] + K_1K_2}$$

138 Eq. 1

$$139 \quad [\text{CO}_3^{2-}] = C_T \frac{K_1K_2}{[\text{H}^+]^2 + K_1[\text{H}^+] + K_1K_2}$$

140 Eq. 2

141 Where [HCO₃⁻] is molar HCO₃⁻; [CO₃²⁻] is molar CO₃²⁻; C_T is molar TDIC (the initial
142 amount of HCO₃⁻ and CO₃²⁻ put into solution as a NaHCO₃ and Na₂CO₃ salt); K₁ and K₂ are

143 temperature-dependent equilibrium constants that account for the dissociation of H_2CO_3 and
144 HCO_3^- , respectively; and $[\text{H}^+]$ is molar hydrogen ions.

145 For solutions prepared as an open system, HCO_3^- and CO_3^{2-} concentrations were
146 calculated based on the open system equations⁵⁶:

$$147 \quad [\text{HCO}_3^-] = \frac{K_1 K_{\text{CO}_2} p\text{CO}_2}{[\text{H}^+]} \quad \text{Eq. 3}$$

$$149 \quad [\text{CO}_3^{2-}] = \frac{K_1 K_2 K_{\text{CO}_2} p\text{CO}_2}{[\text{H}^+]^2} \quad \text{Eq. 4}$$

151 K_{CO_2} (i.e., Henry's constant) is the temperature-dependent equilibrium constant that
152 accounts for the aqueous solubility of CO_2 . When estimating carbonate species concentrations
153 for the calibrations, the equilibrium constants were adjusted to the measured temperature values
154 using the calculations of Drever (1997)⁵⁶.

155 We used the closed system calculations to estimate $p\text{CO}_2$ in natural fluid inclusions,
156 because the trapped solute acts as a closed system post-entrapment and the components of the
157 fluid (alkalinity, TDIC, pH, and $p\text{CO}_2$) are fixed. However, the fluid inclusion would represent
158 the environment pre-entrapment as the solute was equilibrated with the atmosphere, assuming
159 the mineral formed at the Earth's surface. Therefore, fluid inclusions behave as a closed system
160 and estimations of $p\text{CO}_2$ should use such equations.

161 Closed system estimations of $p\text{CO}_2$ require information on $[\text{CO}_3^{2-}]$, $[\text{HCO}_3^-]$, $[\text{CO}_2 \text{ aq}]$,
162 and pH. Our calibrations can quantify $[\text{CO}_3^{2-}]$, $[\text{HCO}_3^-]$, and pH, but estimating $[\text{CO}_2 \text{ aq}]$ must be

163 calculated because its concentration is low in the natural range chosen in this study⁵⁵ (Table 2).

164 To estimate $[\text{CO}_2\text{ aq}]$ we use the following equation:

$$[\text{CO}_2\text{ aq}] = [\text{H}^+]^2 \frac{[\text{CO}_3^{2-}]}{K_1 K_2}$$

Eq. 5

167 Which allows for pCO_2 to be estimated from the calculated $[\text{CO}_2\text{ aq}]$:

$$\text{pCO}_2 = \frac{[\text{CO}_2\text{ aq}]}{K_{\text{CO}_2}}$$

Eq. 6

170 To ensure that the range of $[\text{CO}_3^{2-}]$ and $[\text{HCO}_3^-]$ captures a large range of pCO_2 values,
171 theoretical estimations were performed using the carbonate closed system equations (Eq. 1, 2,
172 and 5) and solved for pCO_2 (Fig. 1). These calculations show that the ratio between $[\text{CO}_3^{2-}]$ and
173 $[\text{HCO}_3^-]$, and pH can be used to estimate a wide range of pCO_2 (-4 to 0) values (Fig. 1). The
174 $[\text{CO}_3^{2-}]$, $[\text{HCO}_3^-]$, and pH of the Na_2CO_3 and NaHCO_3 solutions were input into the carbonate
175 closed system equations to calculate the range of potential pCO_2 values. Figure 1 shows that the
176 concentrations we selected for our solutions can be used to estimate a wide range (-4 to 0) of
177 pCO_2 .

178

179 *Evaluating the Effect of the Carbonate Host Mineral*

180 To evaluate whether the host mineral's birefringence affects the calibration curves of
181 solute concentrations and pH in a natural carbonate sample, a cover slip was made from optical
182 grade calcite to simulate the measurement of a calcite-hosted fluid inclusion. Previous research
183 has demonstrated that the host mineral does not affect determination of salt concentrations in

184 calcite when using a confocal Raman Spectrometer^{8,41}. These authors suggest minimizing the
185 effect of the host mineral in Raman spectroscopy micro-fluid inclusion studies by placing the
186 sample at its extinction position. To test this, a piece of optical grade calcite that has the c-axis
187 parallel to surface and free of visible inclusions and defects was used in a subset of
188 measurements to ensure the host mineral does not affect solute quantification. The cover slip was
189 ground to a thickness of ~100 microns and doubly polished to a colloidal silica grade.

190 A comparison of the standard NaHCO_3 and Na_2CO_3 solutions measured by Raman both
191 with and without the addition of a calcite cover slip was performed for each concentration to
192 measure the effect of the host mineral on solute quantification (Fig. 2). To ensure that the desired
193 focal plane was in the solution, before each measurement, the laser was first focused on the
194 surface of the cover slip and then focused down to the underside of the cover slip, and finally
195 focused 100 microns below and into the solution. For solutions without the calcite cover slip, the
196 laser was focused 100 microns below the surface of the solution.

197

198 *Raman Measurement and quantification of CO_3^{2-} and HCO_3^-*

199 Shortly after a solution was mixed and the open system solutions reached equilibrium, 5
200 microliters of solution were placed in a glass concavity slide and analyzed using a WiTec
201 alpha300 R confocal Raman spectrometer utilizing a 532 nm green laser at the Carnegie Institute
202 of Science, Earth and Planets Laboratory⁵⁷. Laser power at the source was 14 mW during each
203 analysis. Measurements were made using a Zeiss 50x objective, a 50 μm aperture, and a 1 cm^{-1}
204 spectral resolution using a Witec UHTS spectrometer system with a 600 grating and an Andor
205 DV400 camera cooled to -59 °C. Additional measurements were made on a Bruker SENTERRA
206 Raman spectrometer at Rensselaer Polytechnic Institute, Department of Earth and Environmental

207 Science. Measurements were integrated for 30 seconds with 3 accumulations and alternated
208 between the solution and the solution with calcite cover slip to minimize any evolution in the
209 solution composition over the course of the analyses. Each component (H_2O , HCO_3^- , and CO_3^{2-}
210 solution with and without the calcite cover slip, and the calcite cover slip alone) used in this
211 study can be broken down into their individual Raman spectra (i.e., H_2O , CaCO_3 , etc. measured
212 independently), and when constructed together, form a spectra that simulates a fluid inclusion
213 (Fig.2).

214 The HCO_3^- anion has a weak Raman scatter, but in alkaline solutions, HCO_3^- is the
215 dominant anion of the carbonate system and has 9 normal, partially polarized Raman modes
216 ^{5,40,58}. The two broad, weak peaks at 634 cm^{-1} and 673 cm^{-1} with the latter representing δCO_2 .
217 The broad mode at 634 cm^{-1} can be deconvoluted into three sub-bands at 630 cm^{-1} , 634 cm^{-1} , and
218 640 cm^{-1} to represent $\gamma\text{CO-H}$ and δHOC . HCO_3^- modes are prevalent at 843 cm^{-1} (γCO_3), 1017
219 cm^{-1} ($\nu\text{C-OH}$), 1312 cm^{-1} ($\delta\text{CO-H}$), 1360 cm^{-1} ($\nu_s\text{CO}_2$), 1630 cm^{-1} ($\nu_{as}\text{CO}_2$), and 2600 cm^{-1} ($\nu\text{CO-}$
220 H)⁴⁰. The Raman bands of CO_3^{2-} have 6 active Raman modes^{5,38}, where weak peaks occur at 684
221 cm^{-1} (ν_4 , in-plane deformation), 885 cm^{-1} (ν_2 , out-of-plane deformation), 1385 cm^{-1} (ν_3 ,
222 antisymmetric stretch C-O), 1435 cm^{-1} , and 1764 cm^{-140} . However, to avoid issues with peak
223 interferences, low intensity signals, and/or mineral fluorescence, the main vibrational mode of
224 HCO_3^- at 1017 cm^{-1} and CO_3^{2-} at 1066 cm^{-1} was used to quantify the amount of $[\text{HCO}_3^-]$ and
225 $[\text{CO}_3^{2-}]$ in solutions as these are the strongest peaks^{5,40}. Calibration solution data was exported in
226 OriginLab (OriginLab Corp., Northampton, MA, USA) where the spectra was background
227 subtracted and the main HCO_3^- and CO_3^{2-} bands were integrated for their cumulative area ($A_{\text{HCO-}}$
228 $3-$ and $A_{\text{CO}_3^{2-}}$). The area of the HCO_3^- and CO_3^{2-} bands were ratioed ($A_{\text{CO}_3^{2-}}/A_{\text{HCO}_3^-}$) as this
229 parameter is reliable in estimating pH, as well as $[\text{CO}_3^{2-}]$, and $[\text{HCO}_3^-]$ as the concentrations are

230 pH dependent (Fig. 1). The ratioed area of the bands, the measured pH, and the calculated
231 $[\text{HCO}_3^-]$ and $[\text{CO}_3^{2-}]$ of calibration solutions are used to build calibration curves which allows us
232 to estimate $[\text{CO}_3^{2-}]$, $[\text{HCO}_3^-]$, and pH of an unknown sample^{38,59}.

233 *Optical Calcite Fluid Inclusion*

234 An Icelandic Spar calcite sample of an unknown origin was used to evaluate the
235 applicability of our calibration's curves to natural carbonate samples. The Icelandic Spar calcite
236 was chosen as a test sample, as it contained an abundance of primary and secondary fluid
237 inclusions spanning a large size range. An inclusion-free portion of the same mineral was used to
238 make the calcite cover slip and provides the best matrix matched sample to test the calibration
239 curves. The fluid inclusions in the Icelandic Spar calcite are predominantly of two phases, vapor
240 and liquid. For demonstration of the success of the calibration technique, a large inclusion that is
241 $\sim 150 \mu\text{m}$ across and $\sim 150 \mu\text{m}$ below the sample surface was analyzed. Measurements were
242 focused on a large $\sim 150 \mu\text{m}$ fluid inclusion because the area of the phases (aqueous or vapor) of
243 interest were larger than the laser spot size ($\sim 1 \mu\text{m}$ or less). Fluorescence from the host calcite
244 makes it increasingly difficult to analyze small inclusions, especially as parameters such as
245 integration time and accumulations are increased. If carbonate species concentrations and pH of
246 the solution are quantified, then the pCO_2 can be determined in a fluid inclusion using equation
247 six⁵⁵. The spectra of the Icelandic Spar calcite were processed and deconvoluted as the
248 calibration solution, as described in the previous section.

249

250 **Results and Discussion**

251 *Calibration Curves*

252 Aqueous bicarbonate and carbonate calibration curves were made for a range of solution
253 to calibrate the Raman spectrometer to quantify carbonate species concentrations and pH and to
254 investigate the effects of the host mineral and salinity on carbonate species and pH
255 quantification.

256 Area ratio calibrations for standard solutions (without NaCl) with and without the calcite
257 cover slip are similar (Fig. 3 and Table 3; consult this table for equations). Quantification of
258 $[\text{CO}_3^{2-}]$, $[\text{HCO}_3^-]$, and pH using $A_{\text{CO}_3^{2-}}/A_{\text{HCO}_3^-}$ show a power, linear, and exponential
259 relationship, respectively, with and without the calcite cover slip (Fig. 3). NaCl wt% calibration
260 curves display a spreading pattern for $[\text{CO}_3^{2-}]$ and pH estimations with increasing salinity,
261 whereas $[\text{HCO}_3^-]$ have similar slopes and intercepts (Fig. 4 and Table 4; consult this table for
262 equations). Quantification of $[\text{CO}_3^{2-}]$, $[\text{HCO}_3^-]$, and pH using $A_{\text{CO}_3^{2-}}/A_{\text{HCO}_3^-}$ with increasing
263 salinity shows a power, linear, and exponential relationship, respectively.

264 *Characterization of the Raman spectra*

265 The solutions with the calcite cover slip have a peak at 1088 cm^{-1} that may interfere with
266 CO_3^{2-} in solution and can pose a potential problem in accurately quantifying carbonate species at
267 low concentrations in fluid inclusions, as discussed in Dubessy et al. (1992)¹². However, the
268 confocal Raman spectrometer also detects a low CaCO_3 peak at 1088 cm^{-1} that does not interfere
269 with the CO_3^{2-} signal (Fig. 2). With this, the calcite cover slip has little to no effect on estimating
270 $[\text{CO}_3^{2-}]$, $[\text{HCO}_3^-]$, and pH of the system when using area ratio between the carbonate species. At
271 lower concentrations, HCO_3^- and CO_3^{2-} becomes harder to distinguish from the background (pH
272 $= <7$) and perhaps an additional extrapolation scheme may be needed.

273 Caumon et al. (2015)⁴¹ demonstrated that if the crystal symmetry and optical properties
274 are not accounted for then quantification errors can occur. However, this is not a concern in our

275 analyses because we employ a confocal Raman spectrometer which bypasses the calcite cover
276 slip as it is above the focal point and does not contribute to the analysis^{34,60}. Given this, there is
277 no substantial difference expected, and accordingly little effect is observed on the calibration
278 curves between non- and calcite cover slip analyses (Fig. 3). The confidence intervals indicate no
279 major differences between non-calcite cover slip and calcite cover slip as they overlap one
280 another (Table 3).

281 The effects of salinity on the calibrations at low $[\text{CO}_3^{2-}]$ and pH is likely negligible
282 ($[\text{CO}_3^{2-}] < 0.01$ molar and ~ 9.5 pH) (Fig. 4). However, accounting for salinity in estimating
283 $[\text{HCO}_3^-]$ is likely minor at all concentrations as the slope of the calibrations for different
284 salinities overlap within their respective confidence intervals (Fig. 4 and Table 4). Therefore, it
285 may be unnecessary to account for the effects of salinity for a solution at low concentrations
286 (e.g., seawater) and pH in natural fluid inclusions. Although, at higher $[\text{CO}_3^{2-}]$ and pH, salinity
287 should be considered by using the OH^- Raman stretch to quantify the concentration of NaCl ^{6,8}.
288 Their methods to determine NaCl concentration can be applied to natural fluid inclusions to
289 allow for accurate $[\text{CO}_3^{2-}]$, $[\text{HCO}_3^-]$, and pH estimates using our calibrations. Overall, the
290 relationships observed are a promising approach towards accurately quantifying carbonate
291 species and pH to estimate pCO_2 in natural samples.

292 *Measurement of fluid inclusion in Calcite*

293 The results of measurements of the aqueous and gaseous phases of a ~ 150 microns fluid
294 inclusion in the Icelandic Spar calcite are shown in Figure 5. The inclusion formed in an area of
295 the crystal that showed no signs of fracture healing or continual mineral growth along a growth
296 plane⁶¹. Because the origin, internal pressure, density, and temperature of formation of the fluid
297 inclusion is unknown, this section and the measurements described within are presented as a

298 demonstrative proof of concept. We chose this sample for its ample size. Given this, the density
299 of the gaseous phase CO₂ can be determined by using the Fermi diad peak difference (v_1-2v_2) of
300 CO₂^{62,63}. It is worth noting that although fluid inclusion homogenization experiments can be used
301 to determine temperature of formation, it is beyond the scope of this study.

302 In the aqueous phase spectra, the distinctive peaks of the calcite host mineral can be
303 observed as well as a HCO₃⁻ and CO₃²⁻ peak at 1017 cm⁻¹ and 1066 cm⁻¹, respectively (Fig. 5).
304 The OH⁻ stretch is present between 2750-3700 cm⁻¹. The salinity in the fluid inclusion was
305 estimated to be 19.9 wt% using the equation of Wang et al. (2013), assuming that NaCl only is
306 present in solution⁶⁴. The area between the HCO₃⁻ and CO₃²⁻ peaks were calculated, ratioed, and
307 applied to the calibration curves without the calcite cover slip. pH was estimated to be 9.33 ±
308 0.29, and [HCO₃⁻] and [CO₃²⁻] were determined to be 0.044 ± 0.027 and 0.098 ± 0.1 molar,
309 respectively (Table 5). The dissociation and solubility constants were adjusted to the measured
310 salinity value using the calculations of Millero (2006)⁵³ and Onda et al. (1970)⁵⁴. 20C° was
311 assumed for the solubility and dissociation constants to calculate pCO₂ because the temperature
312 at the time of formation is unknown. With carbonate concentrations and solution pH estimated,
313 pCO_{2(g)} was calculated to be -3.78 ± 0.03 (167 ± 13 ppm).

314 In the gaseous phase spectra, the CO₂ Fermi diad is present at 1287 cm⁻¹ and 1389 cm⁻¹,
315 hydrogen sulfide and methane are also present at 2611 cm⁻¹ and 2917 cm⁻¹, respectively⁵ (Fig. 5).
316 The density of CO₂ is essentially zero as the fermi diad technique can be utilized as low as 0.1
317 g/cm^{362,63}. However, the density of present-day atmospheric CO₂ is 0.0019 g/cm³, potentially
318 suggesting that the fluid inclusion formed in an atmosphere between <0.0019 and <0.1 g/cm³ of
319 CO₂. In addition, the lack of major atmospheric gases (e.g., O₂ and N₂), the presence of H₂S and
320 CH₄ suggest that the fluid inclusion precipitated in a reducing environment.

321

322 *Calibration Limitations*

323 Quantification of $[\text{CO}_3^{2-}]$, $[\text{HCO}_3^-]$, and pH can provide information about the pCO_2 of
324 formation of a carbonate fluid inclusion, and there is no observed effect from the host mineral on
325 estimating pH and carbonate species when using a confocal instrument (Fig. 3)^{8,41}. However,
326 there are limitations using this method, including: (1) the Raman spectrometer was calibrated at
327 low temperatures and pressures (1 atm), where it is likely the calibrations will deviate at higher
328 temperatures and pressures as the solubilities and the dissociation constants of the carbonate
329 species change^{65,66}. (2) The calibrated Raman spectrometer does not encompass the low pH
330 range present in modern^{48,52} and ancient systems⁴⁶ (e.g., acidic springs and soils). (3)
331 Determining the alkalinity of fluid inclusions may be impossible with current technology as
332 titrating them would lead to fluid contamination. However, it is reasonable to assume that the
333 alkalinity would be controlled by TDIC, as it is in the modern oceans⁶⁷. (4) Salts (e.g., MgCl_2 ,
334 CaCl_2 , and KCl) are likely to be present in natural carbonate fluid inclusions that will skew the
335 water peaks^{8,64} and may affect accurate determination of pH and species concentrations. (5)
336 Analyses of fluid inclusions are based on small amounts of solution, and this limits the
337 determination of carbonate species concentrations and pH, as a relationship exists between the
338 intensity and the number of molecules present in the sample⁶⁸. For example, if there is a limited
339 amount of water in a carbonate fluid inclusion, a lower intensity water peak will be observed,
340 and as a consequence of this, the HCO_3^- and CO_3^{2-} peaks may not be detectable in these
341 inclusions. However, larger carbonate fluid inclusions are promising as more solution is present
342 and may be able to detect HCO_3^- and CO_3^{2-} (Fig. 5).

343 *Other Applications*

344 The different proxies to estimate pCO₂ in deep time do not agree with one another^{16,23–25}.
345 For example, data from δ¹³C of paleosol carbonates and stomatal indices of fossil plants from the
346 end-Triassic extinction show a corroborating pCO₂ trend, but the absolute pCO₂ values do not
347 agree^{26–28}. One reason is the soil productivity parameter (S(z)) within the soil diffusion model²⁵.
348 This parameter is the concentration of CO₂ in the soil derived from the respiration of organic
349 matter and CO₂ in the atmosphere. CO₂ estimations within a soil is largely unknown and
350 unconstrained because this parameter will fluctuate depending on soil profile depth and soil
351 type¹⁶. However, the calibration presented in this study is a potential method that can constrain
352 the S(z) and estimate pCO₂ within a soil column.

353 **Conclusion**

354 We demonstrate the calibration of a confocal Raman spectrometer over a range of [CO₃²⁻
355], [HCO₃⁻], and pH, representative of natural waters. These calibrations allow for the
356 quantification of carbonate species concentrations and pH in fluid inclusion at low-temperatures
357 and pressures. Calibrations can be used to calculate [CO₃²⁻], [HCO₃⁻], and pH, which ultimately
358 allows pCO₂ to be determined in mineral fluid inclusions, assuming the mineral formed at the
359 Earth's surface and equilibrated with its environment. The host mineral's crystal optics have
360 little to no effect on determining the [CO₃²⁻], [HCO₃⁻], and pH if the Raman spectrometer is
361 confocal. Negligible effects of salinity occur at low [CO₃²⁻] and pH, and all [HCO₃⁻].
362 Homogenization temperature experiments should be conducted in conjunction with confocal
363 Raman experiments to determine accurate pCO₂ estimations in natural fluid inclusions.

364 **Acknowledgements**

365 This research was supported by NASA Earth First Origins grant A129942527. We would
366 like to thank Oliver Wolfe, Samantha Pyror, Nikos Sitaras, Sebastian Barkett, Mikayla Berman,

367 Kristin Johnson-Finn, Jacob Shelley, Frank Spear, and Kristen Chياما for enlightening
368 discussions, edits, and feedback that greatly improved this manuscript. The authors thank the
369 anonymous reviewers for their valuable feedback, and suggestions that greatly improved the
370 quality of the manuscript.

371 **Declaration of Conflicting Interest**

372 The authors declare that there is no conflict of interest.

373 **References**

- 374 1. R.H. Goldstein. “Clues from Fluid Inclusions”. *Science. American Association for the*
375 *Advancement of Science*, 2001. 294(5544): 1009–1011. 10.1126/science.1066322.
- 376 2. E. Roedder. “Introduction to Fluid Inclusions”. *Mineralogical Society of America*. 1984. 12:
377 1–10.
- 378 3. R.J. Bodnar. Chapter 4. *Introduction to Aqueous-Electrolyte Fluid Inclusions*. Mineral.
379 Assoc. Canada, 2003.
- 380 4. L.W. Diamond. Chapter 3. *Systematics of H₂O Inclusions*. Mineral. Assoc. Canada, 2003.
- 381 5. M.L. Frezzotti, F. Tecce, A. Casagli. “Raman spectroscopy for fluid inclusion analysis”.
382 *Journal of Geochemical Exploration*. 2012. 112: 1–20. 10.1016/j.gexplo.2011.09.009.
- 383 6. T.P. Mernagh, A.R. Wilde. “The use of the laser Raman microprobe for the determination of
384 salinity in fluid inclusions”. *Geochimica et Cosmochimica Acta*. 1989. 53(4): 765–771.
385 10.1016/0016-7037(89)90022-7.
- 386 7. T.K. Lowenstein, M.N. Timofeeff, S.T. Brennan, L.A. Hardie, R.V. Demicco. “Oscillations
387 in Phanerozoic Seawater Chemistry: Evidence from Fluid Inclusions”. *Science. American*
388 *Association for the Advancement of Science*, 2001. 294(5544): 1086–1088.
389 10.1126/science.1064280.
- 390 8. Q. Sun, L. Zhao, N. Li, J. Liu. “Raman spectroscopic study for the determination of Cl⁻
391 concentration (molarity scale) in aqueous solutions: Application to fluid inclusions”.
392 *Chemical Geology*. 2010. 272(1–4): 55–61. 10.1016/j.chemgeo.2010.02.004.
- 393 9. T. Azbej, M.J. Severs, B.G. Rusk, R.J. Bodnar. “In situ quantitative analysis of individual
394 H₂O–CO₂ fluid inclusions by laser Raman spectroscopy”. *Chemical Geology*. 2007. 237(3–
395 4): 255–263. 10.1016/j.chemgeo.2006.06.025.
- 396 10. Brigitte. Wopenka, J.Dill. Pasteris. “Raman intensities and detection limits of geochemically
397 relevant gas mixtures for a laser Raman microprobe”. *Anal. Chem*. 1987. 59(17): 2165–2170.
398 10.1021/ac00144a034.
- 399 11. J. Dubessy, B. Poty, C. Ramboz. “Advances in C-O-H-N-S fluid geochemistry based on
400 micro-Raman spectrometric analysis of fluid inclusions”. *European Journal of Mineralogy*.
401 1989. 1(4): 517–534.

- 402 12. J. Dubessy, M.-C. Boiron, A. Moissette, C. Monnin, N. Sretenskaya. “Determination of
403 water, hydrates and pH in fluid inclusions by micro-Raman spectrometry”. *European Journal*
404 *of Mineralogy*. 1992. 4: 885–894. 10.1127/ejm/4/5/0885.
- 405 13. E.A.J. Burke. “Raman microspectrometry of fluid inclusions”. *Lithos*. 2001. 55(1): 139–158.
406 10.1016/S0024-4937(00)00043-8.
- 407 14. M.L. Frezzotti, J. Selverstone, Z.D. Sharp, R. Compagnoni. “Carbonate dissolution during
408 subduction revealed by diamond-bearing rocks from the Alps”. *Nature Geosci.* Nature
409 Publishing Group, 2011. 4(10): 703–706. 10.1038/ngeo1246.
- 410 15. U. Brand, N. Blamey, C. Garbelli, E. Griesshaber, R. Posenato, L. Angiolini, et al. “Methane
411 Hydrate: Killer cause of Earth’s greatest mass extinction”. *Palaeoworld*. 2016. 25(4): 496–
412 507. 10.1016/j.palwor.2016.06.002.
- 413 16. T.E. Cerling. “Stable Carbon Isotopes in Palaeosol Carbonates”. In: M. Thiry, R. Simon-
414 Coinçon, editors. *Palaeoweathering, Palaeosurfaces and Related Continental Deposits*.
415 Blackwell Publishing Ltd., Oxford, UK, 2009. Pp. 43–60. 10.1002/9781444304190.ch2.
- 416 17. M.L. Griffiths, R.N. Drysdale, H.B. Vonhof, M.K. Gagan, J. Zhao, L.K. Ayliffe, et al.
417 “Younger Dryas–Holocene temperature and rainfall history of southern Indonesia from $\delta^{18}\text{O}$
418 in speleothem calcite and fluid inclusions”. *Earth and Planetary Science Letters*. 2010.
419 295(1): 30–36. 10.1016/j.epsl.2010.03.018.
- 420 18. N. Tabor, T. Myers. “Paleosols as Indicators of Paleoenvironment and Paleoclimate”. *Annual*
421 *Review of Earth and Planetary Sciences*. 2014. 43: 150317182938004. 10.1146/annurev-
422 earth-060614-105355.
- 423 19. H.P. Schwarcz, R.S. Harmon, P. Thompson, D.C. Ford. “Stable isotope studies of fluid
424 inclusions in speleothems and their paleoclimatic significance”. *Geochimica et*
425 *Cosmochimica Acta*. 1976. 40(6): 657–665. 10.1016/0016-7037(76)90111-3.
- 426 20. K. Azmy, N.J.F. Blamey. “Source of diagenetic fluids from fluid-inclusion gas ratios”.
427 *Chemical Geology*. 2013. 347: 246–254. 10.1016/j.chemgeo.2013.04.011.
- 428 21. N. Blamey, N.M.I. of Mining, P. Boston, L. Rosales-Lagarde, N.M.I. of Mining, N.S.
429 College. “High-resolution signatures of oxygenation and microbiological activity in
430 speleothem fluid inclusions”. *International Journal of Speleology*. 2016. 45(3): 231–241.
- 431 22. D. Lüthi, M. Le Floch, B. Bereiter, T. Blunier, J.-M. Barnola, U. Siegenthaler, et al. “High-
432 resolution carbon dioxide concentration record 650,000–800,000 years before present”.
433 *Nature*. 2008. 453(7193): 379–382. 10.1038/nature06949.
- 434 23. D.L. Royer, K.M. Moynihan, M.L. McKee, L. Londoño, P.J. Franks. “Sensitivity of a leaf
435 gas-exchange model for estimating paleoatmospheric CO_2 concentration”. *Climate of the*
436 *Past*. Copernicus GmbH, 2019. 15(2): 795–809. 10.5194/cp-15-795-2019.
- 437 24. S.M. Eggins, L.L. Haynes, K.A. Allen, K.D. Holland, K. Lorbacher, B. Hönisch. *Boron*
438 *Proxies in Paleooceanography and Paleoclimatology*. 1st edition. Wiley-Blackwell, Hoboken,
439 NJ, 2019.
- 440 25. D.O. Breecker. “Quantifying and understanding the uncertainty of atmospheric CO_2
441 concentrations determined from calcic paleosols”. *Geochemistry, Geophysics, Geosystems*.
442 2013. 14(8): 3210–3220. 10.1002/ggge.20189.

- 443 26. M.F. Schaller, J.D. Wright, D.V. Kent. “Atmospheric Pco2 Perturbations Associated with the
444 Central Atlantic Magmatic Province”. *Science*. 2011. 331(6023): 1404–1409.
445 10.1126/science.1199011.
- 446 27. M.F. Schaller, J.D. Wright, D.V. Kent, P.E. Olsen. “Rapid emplacement of the Central
447 Atlantic Magmatic Province as a net sink for CO₂”. *Earth and Planetary Science Letters*.
448 2012. 323–324: 27–39. 10.7916/D8PG22B4.
- 449 28. J.C. McElwain, D.J. Beerling, F.I. Woodward. “Fossil Plants and Global Warming at the
450 Triassic-Jurassic Boundary”. *Science*. 1999. 285(5432): 1386–1390.
451 10.1126/science.285.5432.1386.
- 452 29. T.E. Cerling. “Stable Carbon Isotopes in Palaeosol Carbonates”. *Palaeoweathering,
453 Palaeosurfaces and Related Continental Deposits*. Wiley-Blackwell, 2009. Pp. 43–60.
- 454 30. L.W. Diamond. “Review of the systematics of CO₂–H₂O fluid inclusions”. *Lithos*. 2001.
455 55(1–4): 69–99. 10.1016/S0024-4937(00)00039-6.
- 456 31. J.L. Zimmermann, R. Moretto. “Release of water and gases from halite crystals”. *European
457 Journal of Mineralogy*. 1996. 8(2): 413–422.
- 458 32. D.I. Norman, N. Blamey, J.N. Moore. “INTERPRETING GEOTHERMAL PROCESSES
459 AND FLUID SOURCES FROM FLUID INCLUSION ORGANIC COMPOUNDS AND
460 CO₂/N₂ RATIOS”. *Twenty-Seventh Workshop on Geothermal Reservoir Engineering*.
461 2002.
- 462 33. A.E. Williams. “Mass spectrometric analysis of volatiles in fluid inclusions: aliquot
463 calibration valve to simulate inclusion rupture”. *Chemical Geology*. 1996. 131(1): 155–165.
464 10.1016/0009-2541(96)00064-2.
- 465 34. M. Fries, A. Steele. “Raman Spectroscopy and Confocal Raman Imaging in Mineralogy and
466 Petrography”. *Springer Series in Optical Sciences*. 2011. Pp. 111–135. 10.1007/978-3-642-
467 12522-5_6.
- 468 35. J.N. Butler. *Carbon Dioxide Equilibria and their Applications*. Routledge, New York, 1982.
469 10.1201/9781315138770.
- 470 36. T. Hrstka, J. Dubessy, J. Zachariáš. “Bicarbonate-rich fluid inclusions and hydrogen diffusion
471 in quartz from the Libčice orogenic gold deposit, Bohemian Massif”. *Chemical Geology*.
472 2011. 281(3–4): 317–332. 10.1016/j.chemgeo.2010.12.018.
- 473 37. S. Facq, I. Daniel, G. Montagnac, H. Cardon, D.A. Sverjensky. “In situ Raman study and
474 thermodynamic model of aqueous carbonate speciation in equilibrium with aragonite under
475 subduction zone conditions”. *Geochimica et Cosmochimica Acta*. 2014. 132: 375–390.
476 10.1016/j.gca.2014.01.030.
- 477 38. B.G. Oliver, A.R. Davis. “Vibrational Spectroscopic Studies of Aqueous Alkali Metal
478 Bicarbonate and Carbonate Solutions”. *Can. J. Chem*. 1973. 51(5): 698–702. 10.1139/v73-
479 106.
- 480 39. W.W. Rudolph, D. Fischer, G. Irmer. “Vibrational Spectroscopic Studies and Density
481 Functional Theory Calculations of Speciation in the CO₂—Water System”. *Appl Spectrosc*.
482 2006. 60(2): 130–144. 10.1366/000370206776023421.

- 483 40. W.W. Rudolph, G. Irmer, E. Königsberger. “Speciation studies in aqueous HCO₃⁻–CO₃²⁻
484 solutions. A combined Raman spectroscopic and thermodynamic study”. Dalton Trans. The
485 Royal Society of Chemistry, 2008. (7): 900–908. 10.1039/B713254A.
- 486 41. M.-C. Caumon, A. Tarantola, R. Mosser-Ruck. “Raman spectra of water in fluid inclusions:
487 I. Effect of host mineral birefringence on salinity measurement”. Journal of Raman
488 Spectroscopy. 2015. 46(10): 969–976. 10.1002/jrs.4708.
- 489 42. J.D. Frantz. “Raman spectra of potassium carbonate and bicarbonate aqueous fluids at
490 elevated temperatures and pressures: comparison with theoretical simulations”. Chemical
491 Geology. 1998. 152(3): 211–225.
- 492 43. J. Wu, H. Zheng. “Quantitative measurement of the concentration of sodium carbonate in the
493 system of Na₂CO₃–H₂O by Raman spectroscopy”. Chemical Geology. 2010. 273(3): 267–
494 271. 10.1016/j.chemgeo.2010.03.001.
- 495 44. W.W. Rudolph, G. Irmer, E. Königsberger. “Speciation studies in aqueous HCO₃⁻–CO₃²⁻
496 solutions. A combined Raman spectroscopic and thermodynamic study”. Dalton Trans. The
497 Royal Society of Chemistry, 2008. (7): 900–908. 10.1039/B713254A.
- 498 45. Q. Sun, C. Qin. “Raman OH stretching band of water as an internal standard to determine
499 carbonate concentrations”. Chemical Geology. 2011. 283(3): 274–278.
500 10.1016/j.chemgeo.2011.01.025.
- 501 46. K.E. Chave. “Evidence on History of Sea Water from Chemistry of Deeper Subsurface
502 Waters of Ancient Basins¹”. AAPG Bulletin. 1960. 44(3): 357–370. 10.1306/0BDA5FF3-
503 16BD-11D7-8645000102C1865D.
- 504 47. F.T. Mackenzie, R.M. Garrels. “Chemical mass balance between rivers and oceans”.
505 American Journal of Science. American Journal of Science, 1966. 264(7): 507–525.
506 10.2475/ajs.264.7.507.
- 507 48. R.M. Garrels, F. Mackenzie. “Origin of the Chemical Compositions of Some Springs and
508 Lakes”. Am. Chem. Soc. Adv. Chem. Ser. 1967. Pp. 222–242. 10.1021/ba-1967-0067.ch010.
- 509 49. S.D. Burley, J. Mullis, A. Matter. “Timing diagenesis in the Tartan Reservoir (UK North
510 Sea): constraints from combined cathodoluminescence microscopy and fluid inclusion
511 studies”. Marine and Petroleum Geology. 1989. 6(2): 98–120. 10.1016/0264-
512 8172(89)90014-7.
- 513 50. W. Stumm, J.J. Morgan. Aquatic Chemistry: Chemical Equilibria and Rates in Natural
514 Waters. Wiley, 1996.
- 515 51. D. Langmuir. Aqueous Environmental Geochemistry. 1st edition. Prentice Hall, Upper
516 Saddle River, N.J, 1997.
- 517 52. M.E. Sumner, ed. Handbook of Soil Science. 1st edition. CRC Press, Boca Raton, Fla, 1999.
- 518 53. F.J. Millero, T.B. Graham, F. Huang, H. Bustos-Serrano, D. Pierrot. “Dissociation constants
519 of carbonic acid in seawater as a function of salinity and temperature”. Marine Chemistry.
520 2006. 100(1): 80–94. 10.1016/j.marchem.2005.12.001.

- 521 54. K. Onda, E. Sada, T. Kobayashi, S. Kito, K. Ito. "SALTING-OUT PARAMETERS OF GAS
522 SOLUBILITY IN AQUEOUS SALT SOLUTIONS". J. Chem. Eng. Japan / JCEJ. 1970.
523 3(1): 18–24. 10.1252/jcej.3.18.
- 524 55. J.N. Butler. Ionic Equilibrium: Solubility and pH Calculations. John Wiley & Sons, 1998.
- 525 56. J.I. Drever. The Geochemistry of Natural Waters: Surface and Groundwater Environments.
526 Prentice Hall, 1997.
- 527 57. T. Dieing, O. Hollricher. "High-resolution, high-speed confocal Raman imaging".
528 Vibrational Spectroscopy. 2008. 48(1): 22–27. 10.1016/j.vibspec.2008.03.004.
- 529 58. A.R. Davis, B.G. Oliver. "A Vibrational-Spectroscopic Study of the Species Present in the
530 CO₂-H₂O System". Journal of Solution Chemistry. 1972. 1(4): 11.
- 531 59. J.D. Pasteris, O. Beyssac. "Welcome to Raman Spectroscopy: Successes, Challenges, and
532 Pitfalls". Elements. 2020. 16(2): 87–92. 10.2138/gselements.16.2.87.
- 533 60. G. Giridhar, R.R.K.N. Manepalli, G. Apparao. "Confocal Raman Spectroscopy".
534 Spectroscopic Methods for Nanomaterials Characterization. Elsevier, 2017. Pp. 141–161.
535 10.1016/B978-0-323-46140-5.00007-8.
- 536 61. R.H. Goldstein. Chapter 2: Petrographic Analysis of Fluid Inclusions. Mineral. Assoc.
537 Canada, 2003.
- 538 62. K.M. Rosso, R.J. Bodnar. "Microthermometric and Raman spectroscopic detection limits of
539 CO₂ in fluid inclusions and the Raman spectroscopic characterization of CO₂". Geochimica
540 et Cosmochimica Acta. 1995. 59(19): 3961–3975. 10.1016/0016-7037(95)94441-H.
- 541 63. Y. Kawakami, J. Yamamoto, H. Kagi. "Micro-Raman Densimeter for CO₂ Inclusions in
542 Mantle-Derived Minerals". Appl Spectrosc. 2003. 57(11): 1333–1339.
543 10.1366/000370203322554473.
- 544 64. X. Wang, W. Hu, I.-M. Chou. "Raman spectroscopic characterization on the OH stretching
545 bands in NaCl–Na₂CO₃–Na₂SO₄–CO₂–H₂O systems: Implications for the measurement of
546 chloride concentrations in fluid inclusions". Journal of Geochemical Exploration. 2013. 132:
547 111–119. 10.1016/j.gexplo.2013.06.006.
- 548 65. J.J. Carroll, J.D. Slupsky, A.E. Mather. "The Solubility of Carbon Dioxide in Water at Low
549 Pressure". Journal of Physical and Chemical Reference Data. American Institute of Physics,
550 1991. 20(6): 1201–1209. 10.1063/1.555900.
- 551 66. R. Wiebe, V.L. Gaddy. "The Solubility of Carbon Dioxide in Water at Various Temperatures
552 from 12 to 40° and at Pressures to 500 Atmospheres. Critical Phenomena *". J. Am. Chem.
553 Soc. 1940. 62(4): 815–817. 10.1021/ja01861a033.
- 554 67. R.E. Zeebe, D. Wolf-Gladrow. CO₂ in Seawater: Equilibrium, Kinetics, Isotopes. Gulf
555 Professional Publishing, 2001.
- 556 68. M.J. Pelletier. Analytical Applications of Raman Spectroscopy. 1st edition. Blackwell
557 Publishing, Osney Mead, Oxford ; Malden, MA, 1999.
- 558 69. J.A. Hurowitz, D.C. Catling, W.W. Fischer. "High Carbonate Alkalinity Lakes on Mars and
559 their Potential Role in an Origin of Life Beyond Earth". Elements. 2023. 19(1): 37–44.
560 10.2138/gselements.19.1.37.

Figures and Tables

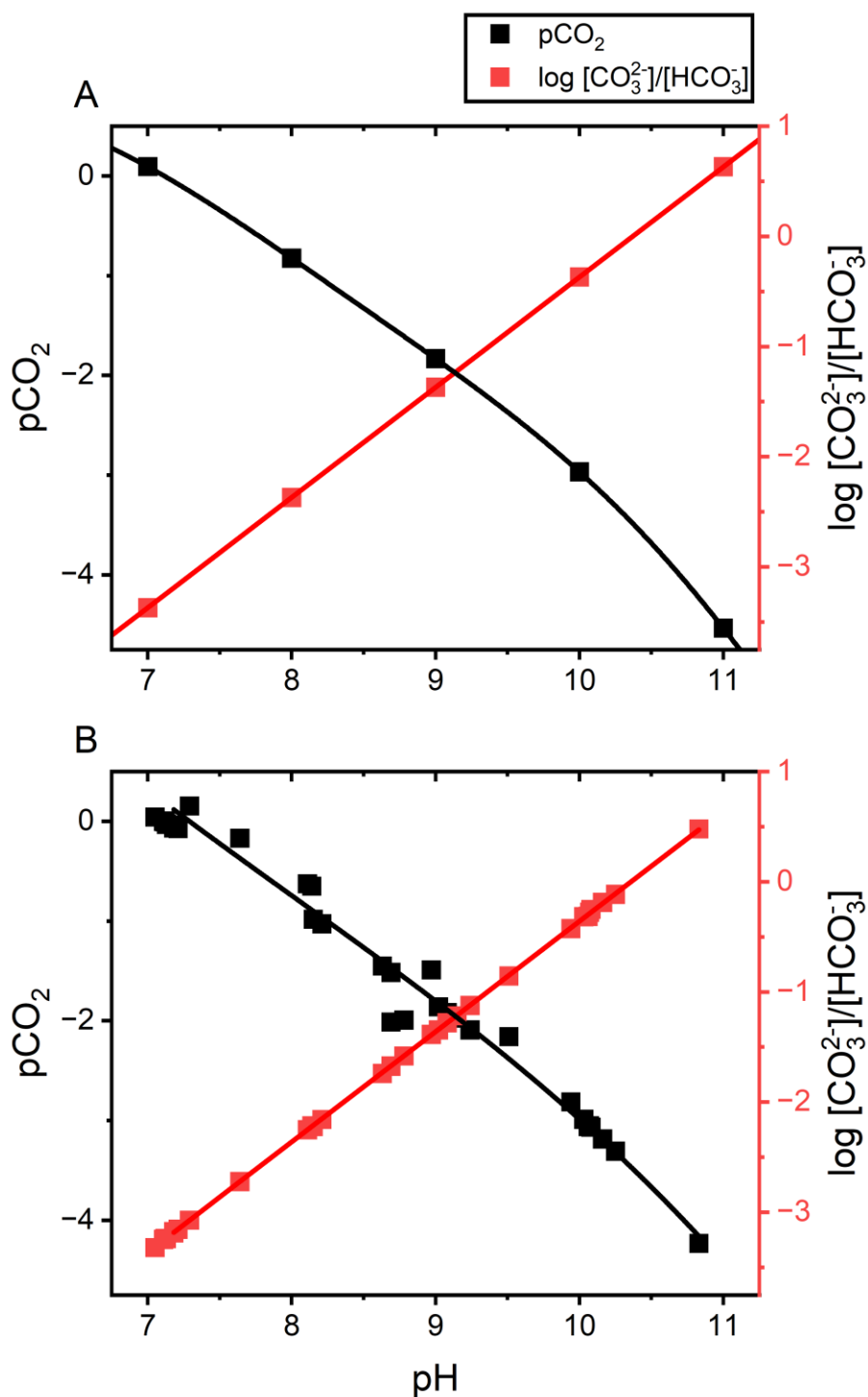


Figure 1. (A) Theoretical calculations of the relationship between the ratio of [CO₃²⁻] and [HCO₃⁻], pH, and pCO₂. The theoretical relationship can be used to estimate pCO₂ over a wide range of alkaline solutions. (B) Solutions used in this study shows the relationship between the ratio of [CO₃²⁻] and [HCO₃⁻], and pH can calibrate for a wide range of pCO₂.

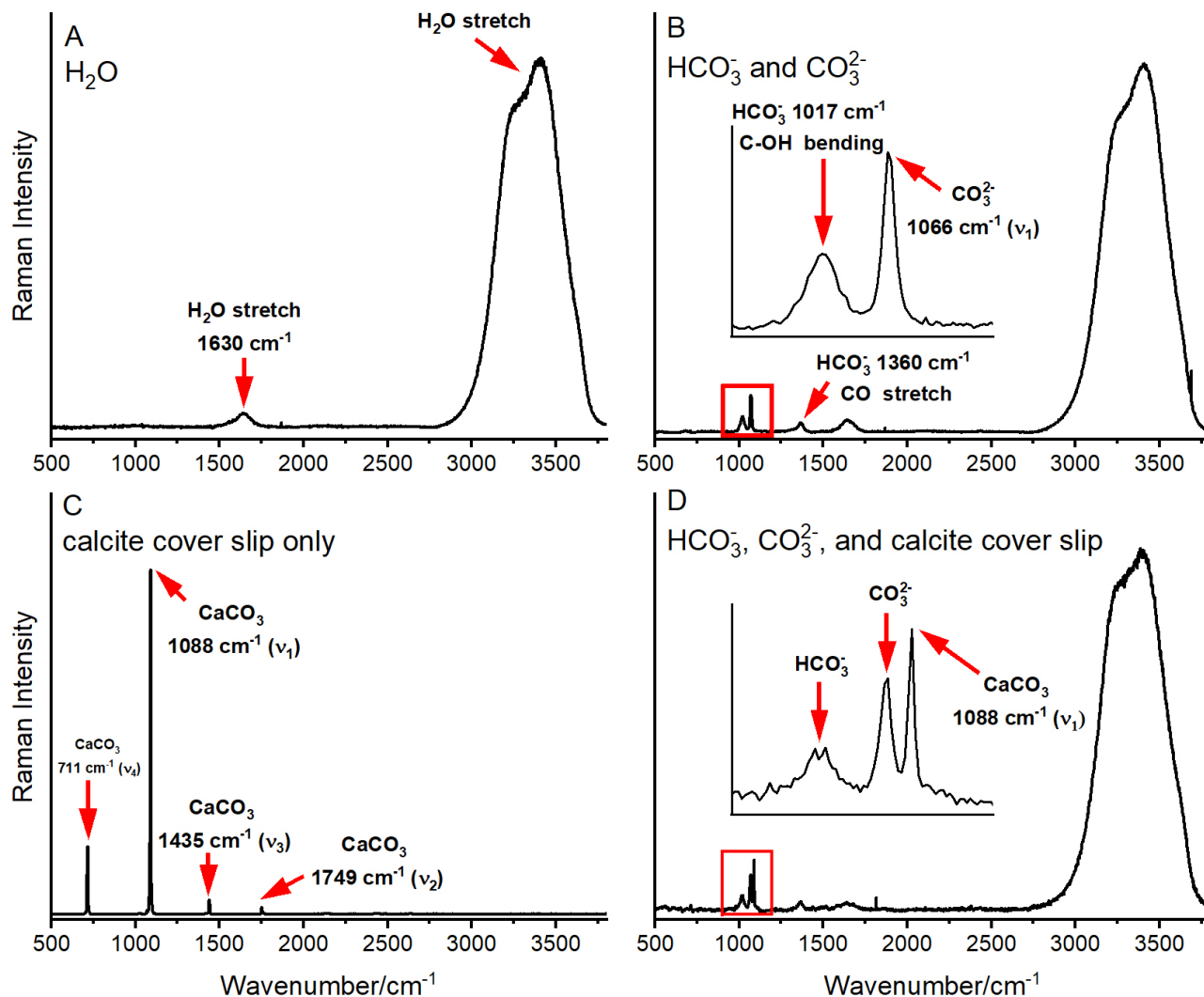


Figure 2. Background corrected Raman spectra of the different components used to build the calibration curves. A) Raman spectra of the Millipore water used to make the solutions. B) Raman spectra of a 0.15 molar NaHCO_3 and 0.03 molar Na_2CO_3 solution with inset of the red box in an area between $950 - 1150 \text{ cm}^{-1}$. The main HCO_3^- and CO_3^{2-} band is at ~ 1017 and $\sim 1066 \text{ cm}^{-1}$, respectively. C) Raman spectra of the calcite cover slip with the main CaCO_3 peak at $\sim 1088 \text{ cm}^{-1}$. D) Raman spectra of the 0.15 molar NaHCO_3 and 0.03 molar Na_2CO_3 solution with the Raman focused $100 \mu\text{m}$ below the calcite cover slip with an inset that shows the respective positions of the HCO_3^- , CO_3^{2-} , and CaCO_3 peaks. Abbreviations: T, translational lattice; ν_1 , symmetric stretching vibration; ν_2 , out-of-plane bending vibration; ν_3 , antisymmetric stretching vibration; ν_4 , in-plane bending vibration.

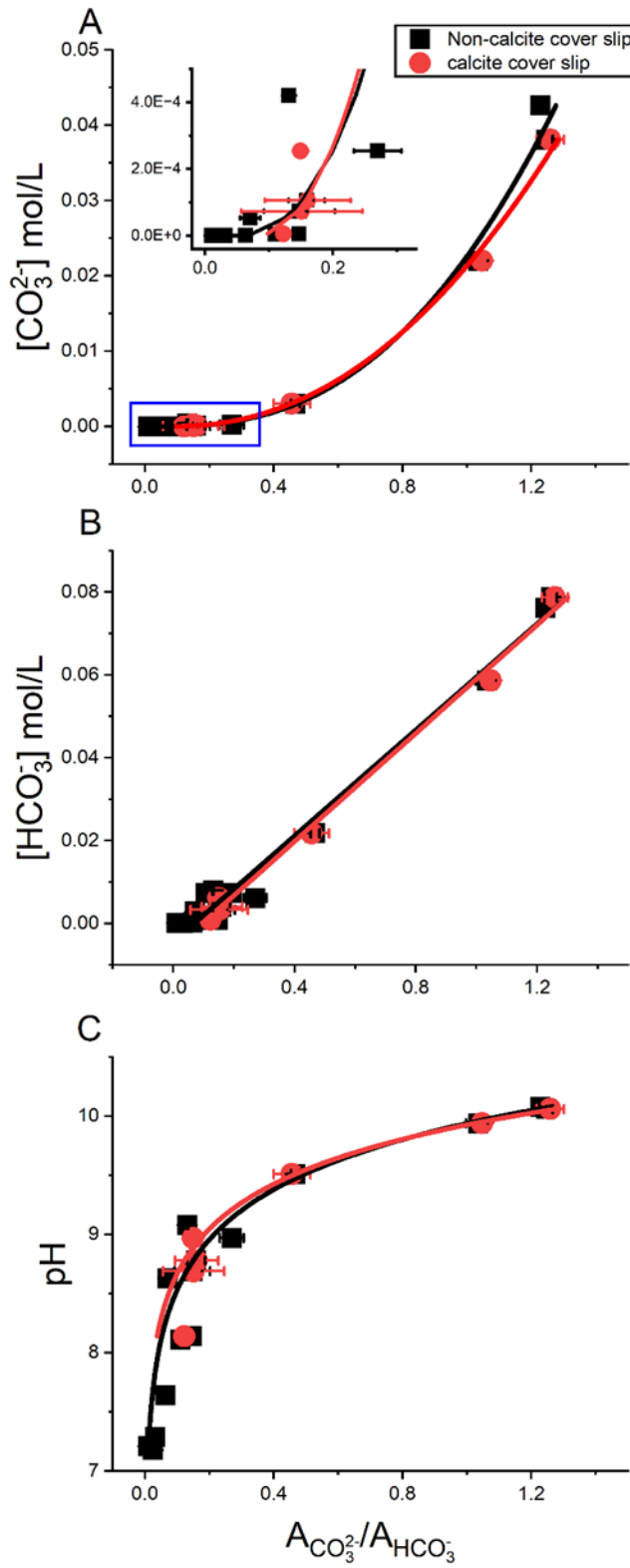


Figure 3. Comparisons of carbonate species concentrations and pH solution calibrations with (red) and without (black) the calcite cover slip. Solution calibrations of $[\text{CO}_3^{2-}]$ (A), $[\text{HCO}_3^-]$ (B), and pH (C) versus the area ratio between CO_3^{2-} and HCO_3^- peaks. Blue box represents the inset within (A). Concentrations are in mol/L.

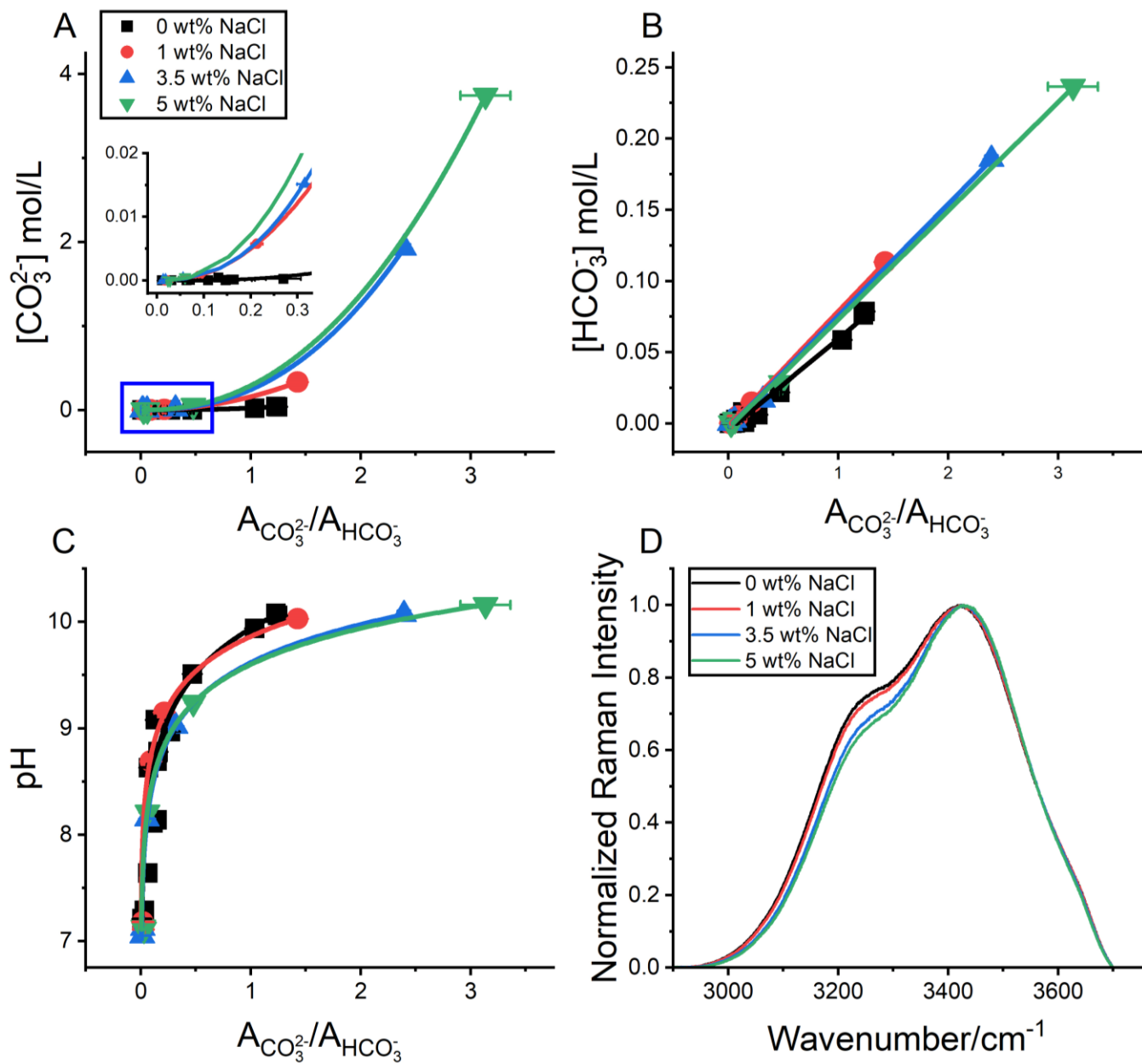


Figure 4. Comparisons of carbonate species concentrations (CO_3^{2-} and HCO_3^-) and pH solution calibrations at various NaCl concentrations (salinities). Solution calibrations of $[\text{CO}_3^{2-}]$ (A), $[\text{HCO}_3^-]$ (B), and pH (C) versus area ratios between the CO_3^{2-} and HCO_3^- peaks. Normalized Raman OH⁻ stretch at different NaCl concentrations. Blue box represents the inset within (A). Concentrations are in mol/L.

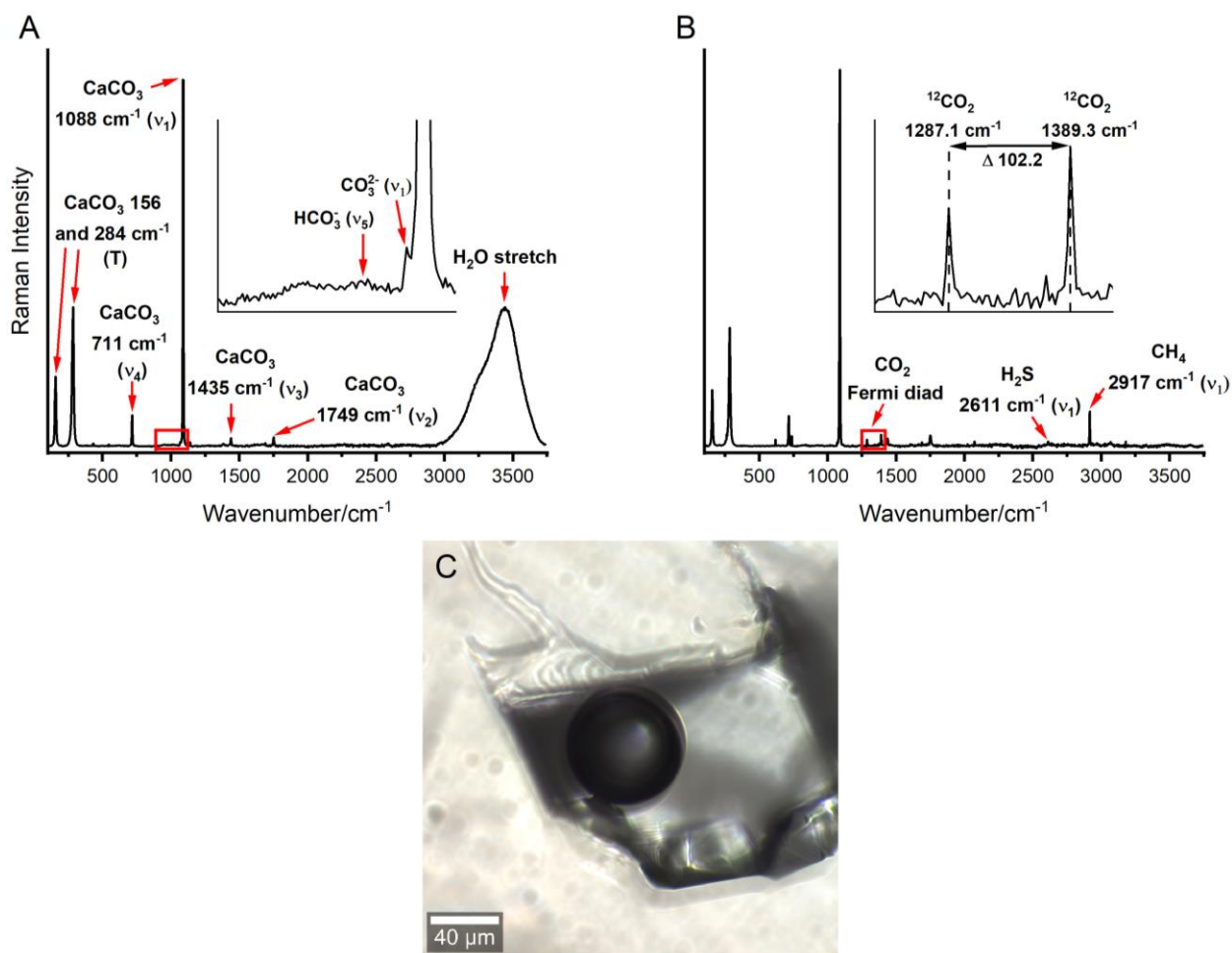


Figure 5. Example Raman spectra of the liquid (A) and gas phase (B) of the large fluid inclusion measured in this study. Liquid phase showing HCO_3^- (1017 cm^{-1}), CO_3^{2-} (1066 cm^{-1}), and H_2O (1630 and $2750\text{--}3750\text{ cm}^{-1}$) peaks with an inset of the red box for the HCO_3^- and CO_3^{2-} peaks. Gas phase shows the CO_2 Fermi diad (1285 and 1388 cm^{-1}), hydrogen sulfide (2611 cm^{-1}), and methane (2917 cm^{-1}). Gas phase inset of the red box shows the CO_2 Fermi diad and the difference between peak distance (Δ) estimates fluid density. Host mineral calcite peaks are present in both in liquid and gas phase spectra at (156 , 284 , 711 , 1088 , and 1435 cm^{-1}). Photomicrograph of the analyzed fluid inclusion in Iceland Spar (C). Abbreviations: T, translational lattice; ν_1 , symmetric stretching vibration; ν_2 , out-of-plane bending vibration; ν_3 , antisymmetric stretching vibration; ν_4 , in-plane bending vibration.

Table 1. Range of carbonate and bicarbonate concentrations (mol/L), and pH in natural waters.

Environment	[CO ₃ ²⁻]	[HCO ₃ ⁻]	pH	Reference
Oceans	0.0002 - 0.0003	0.002 - 0.03	7.4 - 8.3	35,46-48
Rivers	3.6x10 ⁻⁸	0.0005 - 0.002	5.28 - 8.5	35,47,50,69
Groundwater	0.00169	0.0001 - 0.003	5.1 – 10.7	51,52,69
Soil	-	0.0001 - 0.003	4.8 - 10.02	51,52
Fluid Inclusions	-	0.007 - 0.014	-	49

Table 2. Solutions and associated area ratio of carbonate species to water, with and without the calcite cover slip, measured using Confocal Raman spectroscopy.

NaCl wt%	pH	[CO ₃ ²⁻]	[HCO ₃ ⁻]	ACO ₃ ²⁻ /AHCO ₃ ⁻ (non-calcite cover slip)	ACO ₃ ²⁻ /AHCO ₃ ⁻ (calcite cover slip)
0	10.08	0.0426	0.0762	1.228	-
0	10.06	0.0381	0.0787	1.246	1.259
0	9.94	0.0220	0.0587	1.035	1.047
0	9.51	0.0030	0.0218	0.467	0.456
0	9.08	4.2E-04	0.0080	0.131	-
0	8.97	2.5E-04	0.0062	0.270	0.149
0	8.78	1.1E-04	0.0040	0.159	0.160
0	8.69	7.3E-05	0.0034	0.147	0.151
0	8.63	5.3E-05	0.0029	0.071	-
0	8.14	5.6E-06	0.0009	0.146	0.123
0	8.11	4.8E-06	0.0009	0.110	-
0	7.64	5.5E-07	0.0003	0.063	-
0	7.29	1.1E-07	1.3E-04	0.031	-
0	7.21	7.6E-08	1.1E-04	0.010	-
0	7.18	6.7E-08	1.0E-04	0.025	-
1	10.03	0.3326	0.1133	1.425	-
1	9.15	0.0058	0.0149	0.213	-
1	8.69	0.0007	0.0052	0.090	-
1	7.18	6.6E-07	1.6E-04	0.019	-
1	7.11	4.8E-07	1.4E-04	0.022	-
3.5	10.07	1.927	0.1856	2.393	-
3.5	9.02	0.0152	0.0165	0.315	-
3.5	8.15	2.8E-04	2.2E-03	0.055	-
3.5	7.12	2.4E-06	2.1E-04	0.018	-
3.5	7.05	1.7E-06	1.8E-04	0.013	-
5	10.16	3.7454	0.2365	3.134	-
5	9.24	0.0538	0.0284	0.477	-
5	8.21	4.8E-04	0.0027	0.060	-
5	7.13	3.2E-06	2.2E-04	0.023	-
5	7.11	2.9E-06	2.1E-04	0.028	-

Table 3. Results of $[\text{CO}_3^{2-}]$, $[\text{HCO}_3^-]$, and pH estimation correlations with and without the calcite cover slip.

	Test	Equation	R^2	95% CI	RMSE
Non-calcite cover slip	$[\text{CO}_3^{2-}]$	$y = 0.021x^{3.12}$	0.99	0.018-0.023	0.0013
	$[\text{HCO}_3^-]$	$y = 0.064x - 0.004$	0.99	0.059-0.069	0.0035
	pH	$y = \frac{\ln(\frac{x}{8.44 \cdot 10^{-8}})}{1.64}$	0.99	1.42-1.86	0.31
Calcite cover slip	$[\text{CO}_3^{2-}]$	$y = 0.020x^{2.83}$	0.99	0.019-0.021	0.0005
	$[\text{HCO}_3^-]$	$y = 0.065x - 0.006$	0.99	0.060-0.070	0.002
	pH	$y = \frac{\ln(\frac{x}{1.28 \cdot 10^{-8}})}{1.83}$	0.99	1.48-2.18	0.15

Table 4. Results of $[\text{CO}_3^{2-}]$, $[\text{HCO}_3^-]$, and pH estimation correlations at different NaCl wt%.

Test	NaCl wt%	Equation	R ²	95% CI	RMSE
[CO ₃ ²⁻]	1 wt%	$y = 0.16x^{2.14}$	0.99	0.15-0.16	0.0021
	3.5 wt%	$y = 0.24x^{2.39}$	0.99	0.24-0.24	0.0055
	5 wt%	$y = 0.24x^{2.39}$	0.99	0.24-0.24	0.020
[HCO ₃ ⁻]	1 wt%	$y = 0.081x - 0.002$	0.99	0.08-0.082	0.00044
	3.5 wt%	$y = 0.079x - 0.003$	0.99	0.073-0.084	0.0035
	5 wt%	$y = 0.077x - 0.004$	0.99	0.073-0.080	0.0031
pH	1 wt%	$y = \frac{\ln(\frac{x}{7.80 * 10^{-10}})}{2.13}$	0.99	1.9-2.3	0.27
	3.5 wt%	$y = \frac{\ln(\frac{x}{8.26 * 10^{-9}})}{1.93}$	0.99	1.9-2.0	0.025
	5 wt%	$y = \frac{\ln(\frac{x}{3.08 * 10^{-9}})}{2.04}$	0.99	1.93-2.16	0.055

Table 5. Estimated CO₃²⁻ and HCO₃⁻ concentrations (mol/L), pH, pCO₂, and CO₂ (ppm) of the calcite fluid inclusion.

[CO ₃ ²⁻]	[HCO ₃ ⁻]	pH	pCO ₂	CO ₂ (ppm)
0.098 ± 0.1	0.044 ± 0.027	9.33 ± 0.29	-3.78 ± 0.03	167 ± 13